Accepted Manuscript

Investigation into the causes of fracture in railway freight car axle

Zoran Odanovic, Mileta Ristivojevic, Vesna Milosevic-Mitic
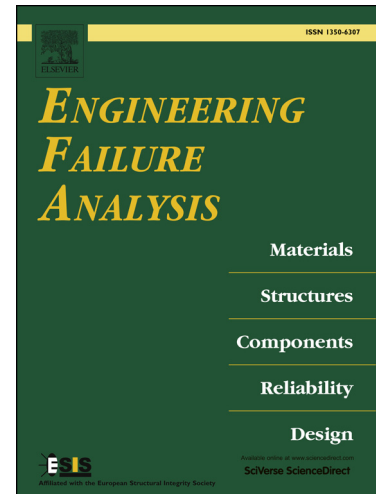
INVESTIGATION INTO THE CAUSES OF FRACTURE
IN RAILWAY FREIGHT CAR AXLE

Zoran**Odanovic**[a]**,** Mileta**Ristivojevic**[b]**,** Vesna **Milosevic-Mitic**[b]

[a] IMS Institute, Bulevar VojvodeMisica 43, 11000 Belgrade, Serbia

[b] University of Belgrade, Faculty of Mechanical Engineering, KraljiceMarije 16, 11120 Belgrade 35, Serbia

Abstract

Railway axles are vital parts of railway. Their failure in the form of dynamic fracture is commonly of disastrous outcomes for railway vehicles. Accordingly, railway axles are designed to be highly reliable, while the maintenance system requires regular inspection in terms of crack initiation. However, due to complex exploitation conditions, complex stress state and multiple stress concentration, railway axles often experience fatigue failures. This occurrence has been studied in a large number of papers. This paper too sheds light on the causes of fracture occurrence in the axle of railway freight car for coal transport in a thermal power plant. Detailed analyses were conducted on the axle fracture surface and mechanical properties. Also, microstructure of the axle material, as well as on exploitation conditions and stress state was examined. Calculations indicated that, apart from working load impact, the influence of press fit joints, especially of the one between the labyrinth seal and the axle is of crucial importance for the analysis of railway axle stress state. The entire numerical-experimental analysis has shown that the considered axle failure was caused by inadequate maintenance, insufficient axle strength and adverse stress state in the railway axle critical cross-sections.

Key words: railway engineering, stress concentrations, failurediagnostics, finite element analysis, non-destructive testing

1.Introduction

Increasing demands for speed and carrying capacity of railway have far reaching effects on working capacity of the vital parts, primarily railway axles, with respect to their reliability and danger of fatigue failure. Railway axles are the most loaded parts of the railway vehicles, which have the most intensive multiple stress concentration. In addition to bending, regular strains, axles can be simultaneously torsional stressed. Those are locomotive's driving axles and disc brake axles. In that case, axles operate as shafts. It has been previously shown in the literature that complex and variable stress state, multiple stress concentration, inadequate maintenance and exploitation conditions, material-related errors and inadequate mechanical properties are the most common causes of failure – fracture of the railway axle-shafts. In [1] a mathematical model was developed for monitoring initial crack growth in railway axles under conditions of variable amplitude loading. Besides theoretical investigations, experimental research was carried out to verify the developed mathematical model. The influence of stress intensity factor on crack formation in railway axle critical cross-sections was analysed in [2]. The analysis was carried out by numerical finite elements method (FEM). Considerations involved stress states at the source of stress concentration located on the bearing journal directly behind the railway wheel as well as on the section of the axle between the railway wheels, with no source of stress concentration. The effects of rotary bending and press fits, at the wheel and gear, on fatigue crack growth and residual lifetime were discussed in [3]. Computational modelling of fatigue crack propagation was presented in [4] and applicable stress intensity factor solution was derived by FEA. The influence of stress fitting on the crack

propagation in a fillet was discussed. In [5] fracture of the driving axle–shaft in the locomotive of the passenger train was analysed. The fracture occurred in the axle-shaft section located between the railway wheels in the cross-section without stress concentration source. It has been shown that the axle-shaft fracture occurred due to a high level of torsional vibrations. Vibrations were generated immediately after the locomotive was set in motion as well as in braking process due to stick-slip phenomenon. In the review paper [6] different forms of destruction in the vital parts of railway are analysed: railway axle-shaft, railway wheel, and rails. A draft procedure for damage tolerance analysis is presented in [7]. As a result of the analysis of the axle, a crack size was provided which has been detected by Non-Destructive Testing (NDT) inspection. One application method of the NASGRO crack growth algorithm to estimate the propagation lifetime of railway axles was presented in [8]. The Paris-Erdogan fatigue crack growth model was found in [9] to be efficient in predicting the fatigue life of the defective railway axle. An overview on safe life and damage tolerance methods applied to railway axles was given in [10]. Some specific features, such as corrosion, which may reduce the fatigue strength of axles were discussed.

The railway axle considered in this paper is the axle of a railway freight car used in the past 35 years, for transportation of coal from the coal mine to the thermal power plant. The axle fracture occurred under exploitation conditions at the source of stress concentration in the cross-section located on the section of the axle between the roller bearing and railway wheel. In order to clarify the cause of this failure, the paper analyses in detail the fracture surface of the axle. Detailed examinations of the mechanical properties and microstructure of the axle material were performed to analyze the effects of the material on the axle fracture. In order to identify potential locations for crack initiations and to evaluate the effects of multiple stress concentration, press fit joints and working load on the axle fracture, the axle stress state was subjected to throughout numerical analysis. Based on numerical calculation (FEM), the axle cross-sections with the highest values of stress were registrated. It has been shown that the most unfavourable stress state is generated in the axle cross-section where the fatigue failure has previously occured. In this study an attempt was made to connect material characterisation results with numerical calculations of the fractured axle, with the aim to improve control and maintenance of the axels in exploitation and to avoid future accidents.

2. Fracture of the railway axle

The freight car for coal transportation from the mine to the thermal power plant has two axles. The failure has taken place on an industrial gauge used for coal transport, as shown in Fig. 1. Under exploitation conditions nominal axle load amounts to 200 kN, while railway car speed of motion is up to 70 km/h. The stopping and braking of railway car is done by brake shoes. Accordingly, under exploitation conditions, the axle is bending stressed only.

Fig. 1. Appearance of damaged railway car

Available data show that the railway axle is regularly periodically inspected and overhauled. However, irrespective of this fact, the axle fracture was detected on the axle assembly journal of the railway rear axle, on the transition radius, on the location of the source of stress concentration, between the roller bearing journal and railway wheel seat. The fracture was not identified on the other end of the axle. The location of the axle fracture is shown in Fig. 2, whereas Fig. 3 represents the journal on the side of the axle where fracture has not occurred.

Fig. 2. Appearance of the railway axle fracture location

Fig. 3. Journal on the side of the railway axle where fracture has not occurred

The available data has shown that the axle was manufactured of unalloyed structural steel which approximately corresponds to C45, according to standard EN 10083. This steel characterises following mechanical properties in normalised condition: Yield strength $R_e \geq 275$ MPa, Tensile strength $R_m \geq 560$ MPa and Elongation $A_5 \geq 16\%$. The axle was designed and manufactured 35 years ago, according to the requirements of the national standard SRPS P.F2.310 (now similar to EN 13261:2003). The investigated axle was manufactured as solid and coated axle. Available user's data shows that similar axle fractures were not evidenced before.

Within the scope of this research in order to identify the cause of axle fracture, following analyses and activities have been undertaken:
- Visual, macrostructural and NDT examination of the fractured axle,
- Chemical composition analyses and mechanical properties testing were conducted in two directions of the axle material,
- Investigation of the microstructure in two directions of the axle material.

A drawing of the solid railway axle with designated fracture cross-section and the testing zone is given in Fig. 4. Working load conditions are identical in both axle fracture cross-section (Fig. 2) and a corresponding cross-section on the other part of the railway axle that has not suffered a fracture (Fig. 3). Accordingly, crack formation should also be expected in this cross-section zone. For that reason this zone has been chosen for testing. The Non-Destructive Testing methods were applied such as Magnetic particle testing and Ultrasonic testing.

Fig.4. Drawing of the tested railway axle with the fracture location and zone examined by the NDT methods

3. Experimental tests. Results and discussion

A detailed experimental testing of the axle material mechanical properties such as tensile properties, impact energy, hardness and microstructural properties was conducted in the longitudinal and transverse direction. A comprehensive analysis of the railway axle stress state was done in order to gain insight of the influence of multiple stress concentration, press fitted joints and working load on the railway axle fracture.

3.1 Visual examination and NDT of the fractured railway axle

In order to determine the cause of the axle fracture visual inspection was performed and the macrostructure of the fracture surface in the axle journal was analysed. Then, NDT methods were applied to examine the presence of cracks in the axle journal where fracture hasn't occurred.
The appearance of the fractured surface of the railway axle is shown in Fig. 5. On the fracture surface a few characteristic zones could be distinguished. The first one is the stress concentration zone around the circumference of the fractured cross section of the axle with tooth like numerous initial cracks of different size. Shape and size of these initial cracks could be explained by observing the appearance of the indications presented in Fig. 6. Numerous initial cracks are formed on the outer surface of the critical axle radius. Due to high stress concentration they were spread parallel to the axle cross section or they were connected and integrated with parallel initial cracks of similar kind. This way they formed specific shape of ratchet, tooth like initial cracks. On these ratchet marks presence of corrosion was evidenced. Next characteristic zones are signed on the Fig. 5 as zone A and B. Appearance of these zones is similar in morphology, but different in shape. It can be concluded that they were initialised at the ratchet marks and propagated by the fatigue

mechanism. These zones are highly oxidised which indicates long presence in axle exploitation. Zone A and B are separated by the radial crack. Based on their deepness it could be concluded that these zones were formed around the same period of the exploitation, but in parallel cross sections of the axle. The static-final axle fracture surface accounts for approx. 30 – 50% of the cross-sectional area and it is a light-coloured surface in Fig. 5 signed as zone C. Generally, it can be concluded that the crack initiations are caused by corrosion pits at the surface of the critical radius of the axle. The newly formed cracks than propagated by the fatigue mechanism until the axle fracture occurred.

Fig. 5. Appearance of the fracture surface with zones characterized by certain types of fracture

Fig. 6. Appearance of cracks registered at the source of the stress concentration location in zone B, where railway axle fracture has not occurred

In order to test the axle material homogeneity at the location of the source of stress concentration, in railway axle zones A and B, where the fracture hasn't occurred (Fig. 4), magnetic particle testing was applied. In the railway axle zone B, surface radial cracks 10 to 160 mm long were detected. The appearance of cracks recorded by the magnetic particle test method on the axle journal radius, where fracture has not occurred in zone B, is shown in Fig. 6. A series of parallel short cracks and an individual crack 160 mm long were detected. An ultrasonic testing was performed at these locations to identify the depth of cracks. These tests indicated that the depths of cracks were up to 30 mm. The reason for formation of cracks with different lengths could be presence of the metallurgical imperfections in the axle material. This means that the eventual presence of the numerous non metallic inclusions in axle cross section could stimulate connection and spreading of the already formed cracks. In the railway axle zone A (Fig. 4), the surface cracks were not recorded. On the basis of the performed non-destructive examinations, it was concluded that further mechanical properties tests and microstructural investigations, with special care at the fracture location, are needed for clarifying reasons for fracture initiation.

3.2. Chemical composition analysis

To view the effects of the axis material on the fatigue failure, chemical composition analysis of the material was performed. Chemical composition was analysed from plate samples prepared according to the standard EN 13261 procedures [11]. Two samples were analysed. One sample was taken from the fracture location and the other one from the non-fracture location. Examinations were done by quantitative spectrophotometric technique, and results are presented in Tab. 1.

Table 1. Results of the axle material chemical analysis (mass. %)

A comparative analysis of the results obtained for chemical composition of the axle material and requirements for rail vehicles specified by standards SRPS P.2.310 and EN 13261:2003 lead to the conclusion that chemical composition of the axle material is compatible with the standard requirements. Only carbon and molybdenum values fall outside the specified limit values.

3.3. Mechanical properties testing

Tensile properties in longitudinal and transverse directions

To perform tensile testing of the axle material mechanical properties, standard test specimens were made and tested in the longitudinal and transverse directions, in compliance with standards EN 13261 and SRPS 10002-1. Test results are presented in Tab. 2. On the basis of comparative results analysis of the axle material mechanical properties (yield strength (R_e) and tensile strength (R_m)) and the requirements for rail vehicles specified by standards SRPS P.F2.310 and EN 13261:2003, it

can be concluded that the axle material tensile properties such as (R_e) and (R_m) are substantially below the recommended standard values. Also, results from the transverse direction tests are unsatisfying. Results of the elongation test for longitudinal direction are according to the corresponding standard requirements. Extreme difference for the elongation and contraction values between the longitudinal and transverse direction are evidenced. Deviation of yield stress from a specified standard value is substantially higher compared to tensile strength deviation.

Table 2. Results of material mechanical properties testing

Additionally, the test results (Tab. 2) indicate heterogeneity with respect to the values of mechanical properties for sampling depth. On the axle surface the values of mechanical properties are the highest, whereas in the vicinity of the axle axis they are the lowest. Specified by the standard SRPS C.B9.021 dynamic propertis of the axle material were: fatigue bending strength of 285 MPa and fatigue tensile strength of 225 MPa.

Impact energy in longitudinal and transverse directions

Impact energy testing of the axle material was performed on standard test specimens in longitudinal and transverse directions, conforming to EN 13261:2003 standard. Test results are given in Tab. 3. The results indicate that the axle material impact energy in longitudinal direction is substantially lower (approximately 30%) than required standard values. Also, impact energy in transverse direction is lower compared to standard values (for 55%).

Table 3. Measured impact energy

Results of hardness testing

Preparation of test pieces for the axle hardness testing was performed at the axle longitudinal cross-section. Hardness was measured at three cross-section levels: on the axle surface, at mid-radius and in the centre of the axle. At each level, hardness was measured at three measuring points. Test results obtained by the Brinell method are presented in Tab. 4. The highest values of hardness are on the axle surface and the lowest in the centre. The differences in hardness values for various testing levels through the axle cross section are not so noticeable as tensile and impact properties differences.

Table 4. Measured material hardness

The results obtained from chemical composition testing indicate that the applied steel used for this type of axles is in accordance with the requirements of the relevant standard.
On the other hand mechanical properties of applied material are below the standard requirements. Applied exploitation conditions of the investigated axle influenced the axle's susceptibility to form initiations for different kind of damages. Low values of the tested mechanical properties could be explained as a result of the insufficiently applied reduction rate in hot rolling/forging process during the axle production, or inadequately applied heat treatment process.

3.4 Metallographic tests

To examine the axle material condition, presence of segregations and/or non-metallic inclusions, grain size and decarburization, and identify possible sources for crack initiation (on macro and micro levels), the corresponding metallographic investigations were conducted using light optical microscopy (LOM).

Macrostructural segregation testing

Segregation testing was performed by macroscopic method using sulphur print (Baumann method). Only small-scale heterogeneities were observed on the examined test piece.

Results of microstructure analysis

Metallographic analysis was done using LOM at magnifications from 100 to 500 times. Testing was performed in both, longitudinal and transversal direction, on the samples from the undamaged part of axle, and near the axle fracture. Sample preparation was performed by classical methods of grinding and polishing. Etching was done with 3% Nital solution.

To examine the contents of non-metallic inclusions the comparing method with reference charts, according to the standard ISO 4967, was applied. Investigations were performed at the three levels of the axle cross section, near the surface, in the mid-radius and in the axle centre.On the basis of the results, it was concluded that non-metallic inclusions of the A, B, C and D type are present in the axle material microstructure. Their sum, in this case, is not greater than specified by standard EN 13261:2003 for A, B and C type. But in the samples gathered from locations near the axle surface and from axle centre, inclusions of type C (silicate) and type D (globular oxide) were identified in the amounts above allowed. Also a few individual coarse non-metallic inclusions of 0.7-1.7 mm long and approximately 20µm in thickness were noted near the axle surface. These coarse non-metallic inclusions are potential sources for cracks initiation and formed cracks could easily propagate through the axle material which has mechanical properties below the required, as it was noticed before. Presence of the non metallic inclusions is illustrated by Fig. 7.

a) longitudinal direction   b) transverse direction
Fig. 7. Non-metallic inclusions near the external surface of the axle

Microstructure analysis was performed on both samples from the transition radius zone and those taken from the vicinity of cross-section at the axle fracture location. The sample was taken from the radius location in the direction of the axle plastic deformation directly at the axle cross-section surface. Sampling location as well as the location on the radius, where decarburization was tested on heat welded metallographic sample is shown in Fig. 8.

Microstructure analysis of the tested material was performed according to the standard EN 13261:2003 requirements. The microstructure of the examined material is banded in the longitudinal direction and ferritic-perlitic microstructure is shown in Fig. 9.

Fig. 8. Sampling location and decarburization-testing location

Fig. 9. Lamellar perlite and ferrite in the axle material microstructure

In the structure, locations with corrosion pits are observed in the material surface layer in the transition radius zone, and in the vicinity of the cross-section where the axle fracture occurred. The presence of corrosion pits is shown in Figs 10 and 11. The size of corrosion pits ranged from approx. 25 to 100 µm in diameter and from 12 to 100 µm in depth. Characteristic corrosion pit is presented in Fig. 10. Corrosion pits were noted to connect with non-metallic inclusions, approx. 100 µm long, which is displayed in Fig. 11.Existing corrosion pits are associated with non metallic inclusion in soft ferritic matrix. Presented corrosion pits could be defined as the potential sites for the crack initiations, and the connection of these pits with evidenced non metallic inclusions enables the crack propagation. The combination of weak axle material, connection and spreading of cracks,

subsequently followed with their propagation cause the fatal fracture of the axle. Pits formation is the result of the damaged axle coat which is evidenced on the both investigated critical radiuses of the axle. As presented before in Fig. 5 and Fig. 6 crack initiations as well as cracks themself were identified on the whole critical radius of the both sides of the axle. This fact leads to the conclusion that corrosion was initiated from the locations of damaged coat, and from below the coat to the whole surface of the critical radius thus creating conditions for pits forming.

Fig. 10. Corrosion pit in the axle material surface layer in the transition radius zone

Fig. 11. Corrosion damage in the material surface layer with subjoined sulphide non-metallic inclusions located in a ferritic band

Grain size was determined according to standard EN ISO 643:2012 using the method of linear segments. The results of grain size index analysis presented in Fig. 9 indicate that grain size is approx. $G = 5$.

Decarburization was tested by the microscopic method. The specimen location for decarburization testing is shown in Fig. 8. The test piece was taken from the radius location in the direction of the axle plastic deformation directly at the axle cross-section surface. Based on the analysis results, it can be concluded that decarburization was not observed in the axle material surface layer on the examined test piece.

4. Analysis of the axle stress state

A detailed analysis of the solid axle stress state was performed in order to analyse the effects of working load, press fit joints and axle geometric characteristics on its fatigue behaviour. Analytical calculations were conducted for the axle mechanical model in the form of the beam with two consoles. The acting load of the axle is the load produced from the transported load mass enlarged by the factor of non-uniform load distribution. On the railway axle consoles, i.e., at the roller bearing location a load is acting in the form of transverse force with the intensity of 130 kN. The axial force of 32.5 kN is generated at the contact between the wheel and rail. Under the action of these loads, the railway axle is stressed in torsion. In addition to these loads, the effects of press fit joints between the wheel and axle, and the bush labyrinth seal and axle on the axle stress state, were observed. The pressure between the bush labyrinth seal and axle amounts to $p_1 = 68$ MPa, and between the wheel and axle $p_2 = 100$ MPa. The analysis of axle stress state has been considered by applying the numerical FEM, which confirmed analytically obtained values of maximal stresses in the axle critical cross-sections.

The first model for FEM calculations [12, 13] was created using volumetric finite elements. A quarter railway axle model with wheels was developed by means of 11 591 points and 9288 finite elements. The conditions of symmetry were specified, as well as a moving support at the wheel-rail contact. Resulting maximal displacement on the axle free end is 1.5 mm and 1.6 mm in the centre of axle. Wheel displacements on the ends range from 2.1 mm on the upper section to 2.5 mm on the lower section (Fig. 12).

Fig. 12. Model, deformation

Fig. 13. Equivalent stress according to the Hencky-Misses hypothesis

The results from Fig. 13 indicate that the highest stresses are generated in the cross-sections at the location of the source of stress concentration. It is the cross-section with the source of stress

concentration located in front of the wheel, Ø 146 (B), where the axle fracture has occurred, and the cross-section with stress concentration located behind the wheel Ø 160 (A). While only vertical force is acting, maximal equivalent stress amounts to 60 MPa in the critical cross-section in front of the wheel and 65 MPa in the critical cross-section behind the wheel. The horizontal force does not affect stress increase, on the locations where axle fracture B has occurred, but it increases stress in the critical cross-section behind the wheel, which then equals 95 MPa.

The next stage involved the analysis of simultaneous effect of loading from the load mass and pressure at the press fit joints location on the axle stress state. This calculation was performed on a quarter railway axle model developed by applying 4641 points and 3600 volumetric finite elements. Also, 288 surface finite elements were fictionally added to the model so that the pressure at the press fit joints locations is more easily specified. The horizontal force was reduced to the axle axis, and then a corresponding moment of the force was added. Figure 14 shows the positions of bush labyrinth seal and wheel.

Fig. 14. Positions of bush labyrinth seal and wheel

First, the comparison with the previous calculations was carried out. The stress state picture of the concentrated stresses is presented in Fig. 15 and obtained values coincide with the values of previously presented calculations. Figure 16 represents the corresponding deformation. Maximal displacement of the axle ends amounts to 1.53 mm coinciding with the previous calculations.

Fig. 15. Equivalent stress according to the Hencky-Misses hypothesis

Fig. 16. Axle deformation

Figure 17 displays stress fields at different combinations of mentioned loads:
- Load 1 - forces and pressures p_1=68 MPa, p_2 = 100 MPa,
- Load 2 - forces and pressure p_1 = 68 MPa (p_2 = 0),
- Load 3 - forces and pressure p_2 = 100 MPa (p_1 = 0).

Fig. 17. Stress fields for different combinations of loads

The analysis of results indicates that pressure p_1 generated in a press fit joint of the railway axle and labyrinth seal affects substantially the stress amount in the railway axle critical cross-section where the fracture has occurred. Without this influence, the highest stresses occur in the cross-section behind the wheel. Due to the action of the pressure p_1, the stress increases in the cross-section where the axle fracture has occurred, in this way it then becomes the axle critical cross-section. Stress distribution in the observed axle cross-sections is shown in Fig. 18.

Fig. 18. Diagrams of stress distribution in the observed cross-sections

It is evident from the diagrams given above that the stress value in the critical cross-section where the axle fracture has occurred, Ø 146 mm, is affected by both pressures, whereas the stresses in the other cross-section are not affected by pressure p_1.

It follows from all presented results that the highest stresses are generated in the axle cross-section where the fracture has occurred. When all mentioned loads are taken into account (forces and pressures), in this cross-section maximal equivalent stress amounts to 105 MPa, and in the cross-section behind the wheel it is 93.7 MPa.
In order to determine the value of pressure p_1, when maximal stresses in the axle critical cross-sections are the same, in front of and behind the wheel, the values of pressures p_1 and p_2 were

varied. Figure 19 shows maximal equivalent stresses in the cross-sections considered at $p_2 = 90/100/110$ MPa. In the presented diagram it is noticeable that when the values of pressure p_1 are larger than 35 MPa, the axle critical cross-section is the one where the axle fracture has occurred.

Fig. 19. Maximal equivalent stress on positions (A) and (B) as a function of p_1

5. Conclusion

On the basis of performed examinations, it has been shown that the values of the axle material mechanical properties, yield stress and tensile strength are substantially lower than the recommended ones. Accordingly, the axle dynamic strength, i.e., the ability of the railway axle to resist the fatigue failure is reduced. Also, the values of impact energy, in the longitudinal and transverse directions, are substantially lower than the recommended ones.

Non-destructive testing has revealed surface cracks in the stress concentration zone where the axle fracture has occurred, as well as in the corresponding zone on the other end of the axle. Due to the less slow propagation of developed cracks, the axle fracture has not occurred. Simultaneously, in the stress concentration zone located behind the wheel surface cracks were not observed. In the axle material, coarse non-metallic inclusions and corrosion pits were registered in the axle surface layer.

Corrosion pits which act like the potential sites for the stress concentration and crack initiations, coupled with evidenced non metallic inclusions enables cracks propagation. Due to the weakness of the material these cracks have propagated, were connected and have spread which led to final fracture of axle.

It has been shown by the axle stress state analysis that maximal stress state under axle exploitation conditions is generated in the axle cross-section where the axle fracture has occurred.

Numerical calculations indicated that stress state is also greatly affected by press fit joints, especially the one between the bush labyrinth seal and axle. It is therefore mandatory to consider the effect of all press fit joints in the analysis of the axle stress state.

In order to prevent the repetition of resulting damage, it is necessary to improve the control of the corrosion protection and the inspection of the axle shaft from the aspect of the initial cracks during the regular maintenance.

Due to inadequate corrosion protection of the axle sections at the location of the source of stress concentration, substantially reduced values of the axle material mechanical properties and presence of non-metallic inclusions, the most stressed axle cross-sections could not transmit the load which generates stress of 105 MPa under exploitation conditions.

Acknowledgment

References

[1] Luke M, Varfolomeev I, Luktepohl K, Esdets A.Fracture mechanices assessment of railway axles: Experimental characterization and computation.Eng. Failure Analysis 2010;17:617-23.
[2] Madia M,Beretta S, Schodel M, Zerbst U, Luke M, Varfolomeev I.Stress intensity factor solutions for craks in railway axles. Engineering Fracture Mechanics 2011;78:764-92.
[3] Madia M, Beretta S, Zerbst U.An investigation on the influence of rotary bending and press fitting on stress intensity factors and fatigue crack growth in railway axels. Engineering Fracture Mechanics 2008;75:1906-20.
[4] Luke M, Varfolomeev I, Luktepohl K, EsdetsA.Fatique crack growth in railway axels: Assessment concept and validation tests.Engineering Fracture Mechanics 2011;78:714-30.

[5]Ognjanovic M, Simonovic A, Ristivojevic M,Lazovic T. Research of rail traction shafts and axles fractures towards impact of service conditions and fatigue damage accumulation. Engineering Failure Analysis 2010;17:1560-71.

[6]Zerbst U, Madler K, Hintze H. Fracture mechanics in railway applications-on overview. Engineering Fracture Mechanics2005;72:163-94.

[7] Zerbst U,Vormwald M, Andersch C, Madler K, Pfuff M.The development of a damage tolerance concept for railway components and its demonstrations for a railway axle. Engineering Fracture Mechanics 2005;72:209-39.

[8] Beretta S, Carboni M. Experiments and stochastic model for propagation lifetime of railwayaxsels, Engineering Fracture Mechanics 2006;73:2627-41.

[9] Torabi A.R, HeidaryKhavas M. Fatique Crack Growth in a Solid Circular Shaft Under Fully Reversed Rotating Bending, J. Fail. Anal.And Preven. 2012;12:419-26

[10] Zerbst U, Beretta S, Kohler G, Lawton A, Vormwald M, BeierH.Th, et al.Safe life and damage tolerance aspects of railway axles - A review. Engineering Fracture Mechanics 2013;98:214-71

[11] EN 13261: Railway applications. Wheelsets and Bogies.Axles.Product requirements.

[12] Maneski T, Milošević-Mitić V.Numerical and experimental diagnostic of structural strength.Structural integrity and life 2010;10(1):3-10.

[13] Zloković GM, Maneski T, Nestorović M. Group theoretical formulation of quadrilateral and hexahedral isoparametric finite elements. Computes & Structure 2004;82(11-12):883-99.

Corresponding author.
E-mail address: vmilosevic@mas.bg.ac.rs (V. Milosevic-Mitic)
Tel. +381 11 3302 237
University of Belgrade, Faculty of Mechanical Engineering, KraljiceMarije 16, 11120 Belgrade 35, Serbia

Fig. 1. Appearance of damaged railway car

Fig. 2. Appearance of the railway axle fracture location

Fig. 3. Journal on the side of the railway axle
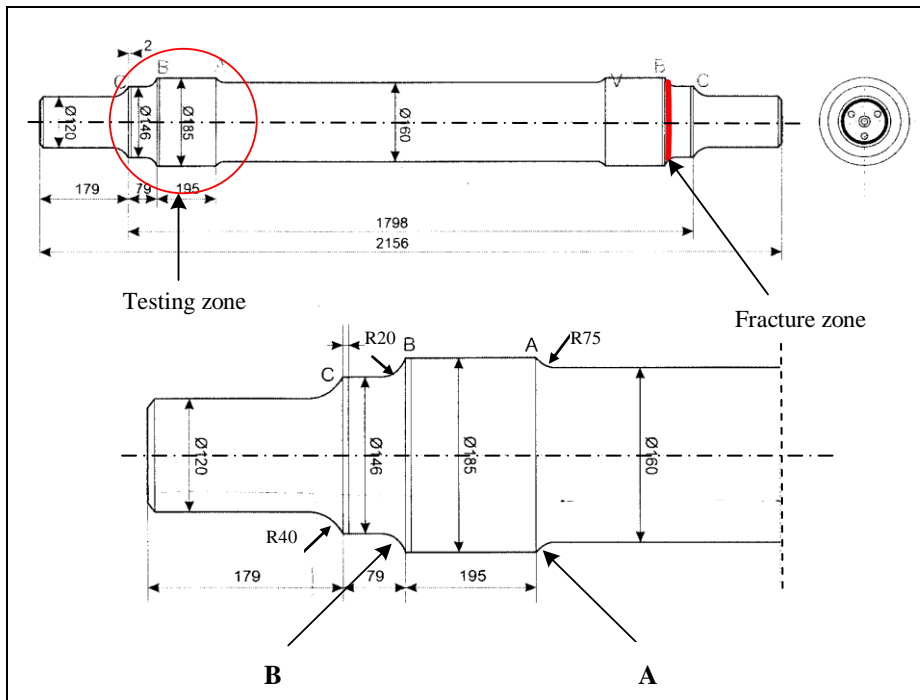where fracture has not occurred

Fig.4. Drawing of the tested railway axle with the fracture location and zone examined by the NDT methods
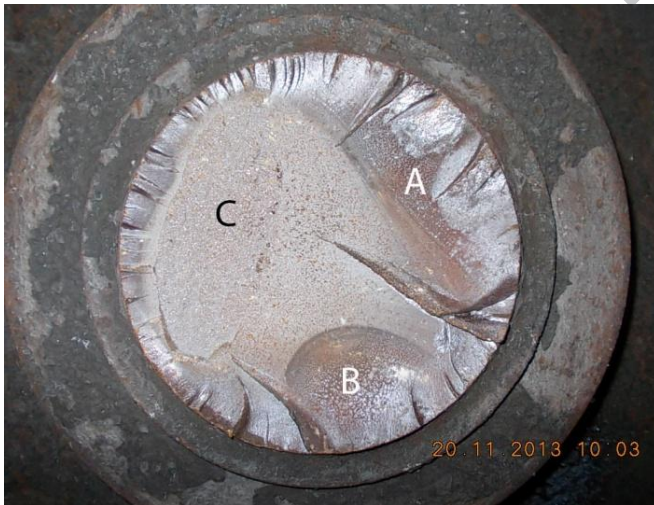

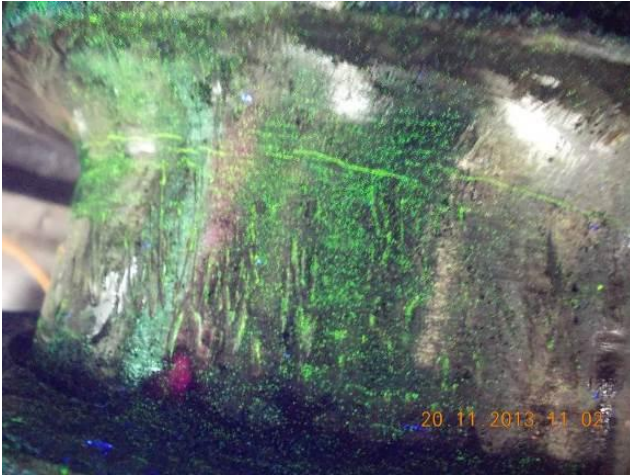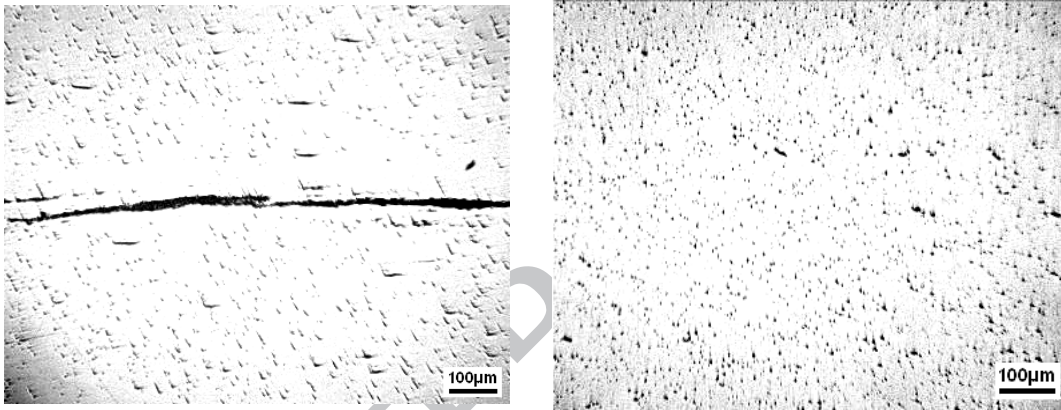**Fig. 5.** Appearance of the fracture surface with zones characterized by certain types of fracture

Fig. 6. Appearance of cracks registered at the source of the stress concentration in zone B where railway axle complete fracture has not occurred

a) longitudinal direction

b) transverse direction

Fig. 7. Non-metallic inclusions near the external surface of the axle
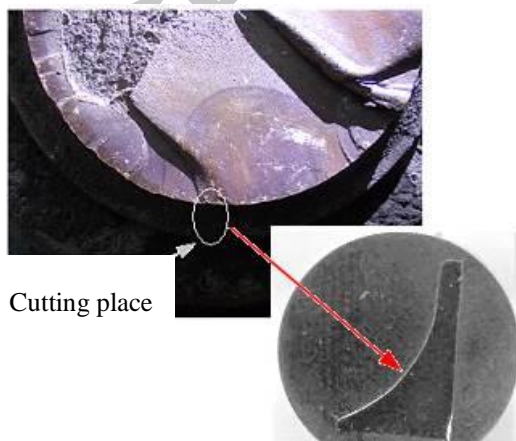
Cutting place

Fig. 8. Sampling location and decarburization-testing location
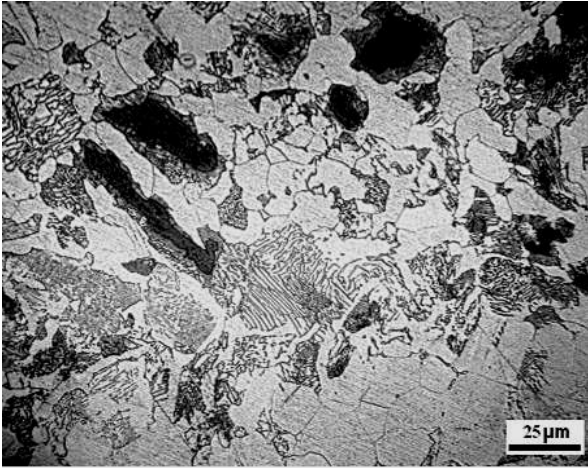
Fig. 9. Lamellar perlite and ferrite in the axle material microstructure
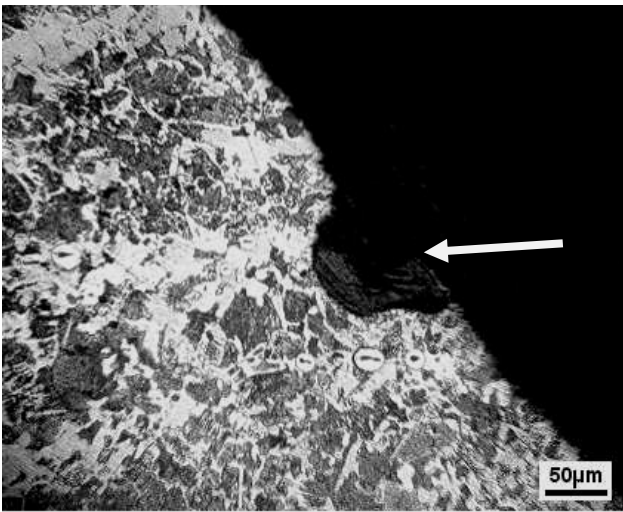
Fig. 10. Corrosion pit in the axle material surface layer in the transition radius zone
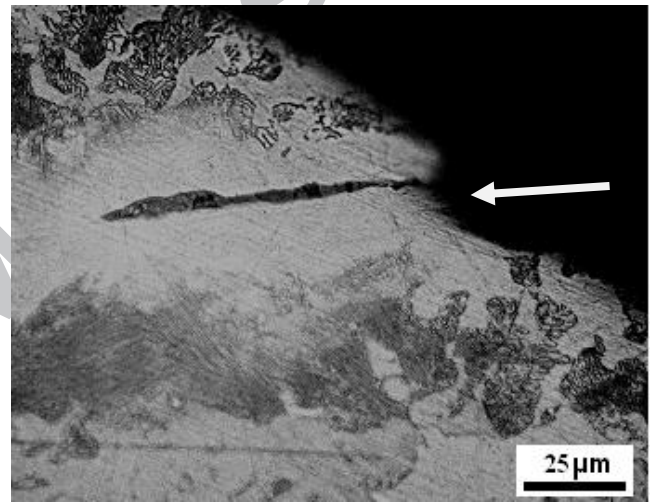
Fig. 11. Corrosion damage in the material surface layer with subjoined sulphide non-metallic inclusions located in a ferritic band
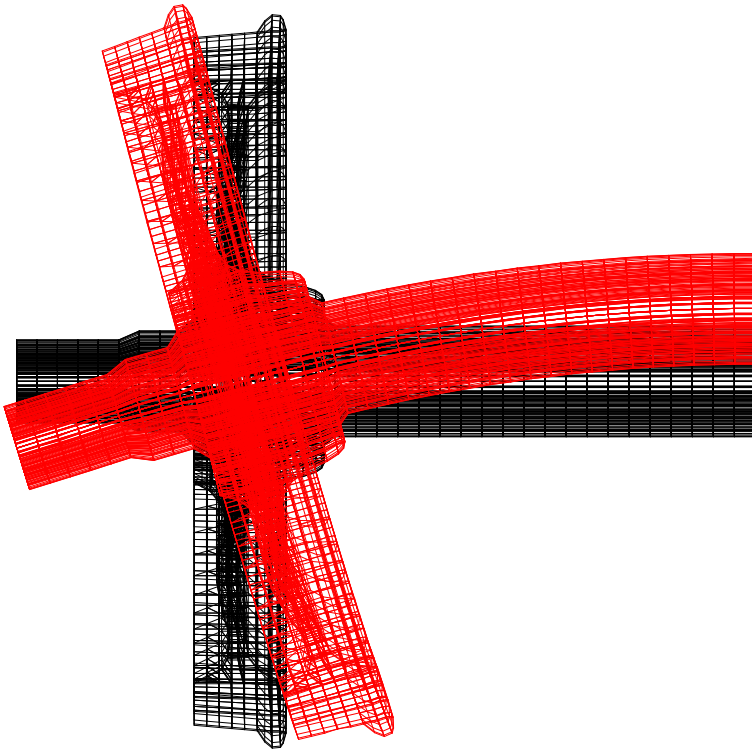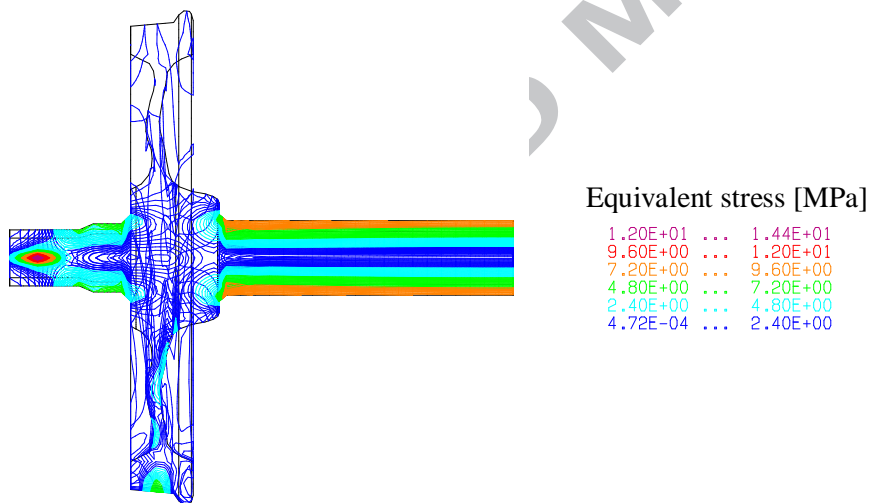
Fig. 12. Model, deformation

Equivalent stress [MPa]

1.20E+01	...	1.44E+01
9.60E+00	...	1.20E+01
7.20E+00	...	9.60E+00
4.80E+00	...	7.20E+00
2.40E+00	...	4.80E+00
4.72E-04	...	2.40E+00

Fig. 13. Equivalent stress according to the Hencky-Misses hypothesis

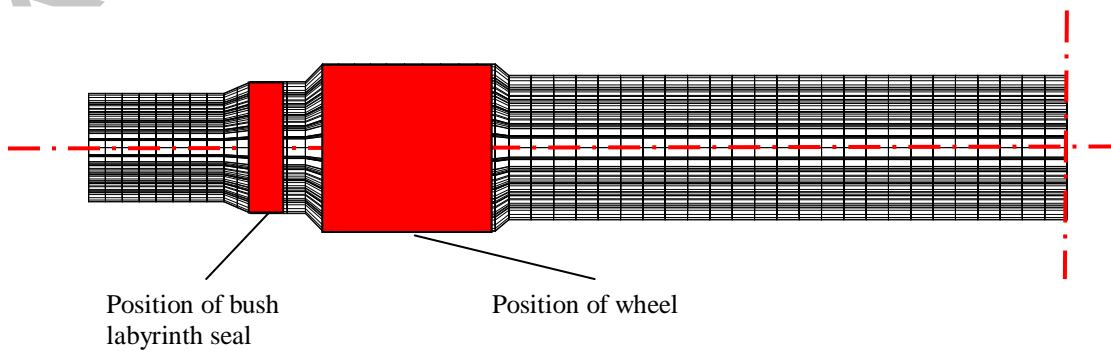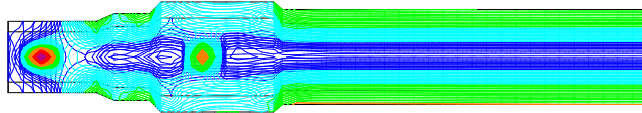Position of bush
labyrinth seal

Position of wheel

Fig. 14. Positions of bush labyrinth seal and wheel

Equivalent stress [MPa]

```
1.32E+02 ... 1.58E+02
1.05E+02 ... 1.32E+02
7.90E+01 ... 1.05E+02
5.27E+01 ... 7.90E+01
2.63E+01 ... 5.27E+01
2.01E-03 ... 2.63E+01
```

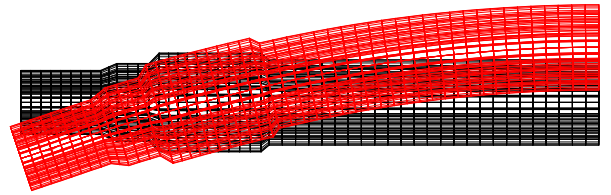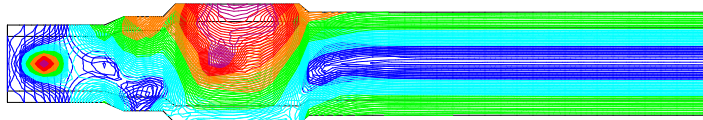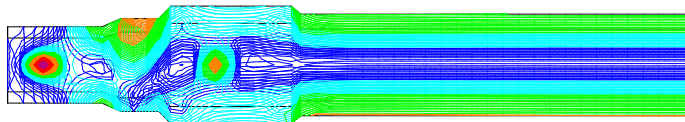**Fig. 15.** Equivalent stress according to the Hencky-Misses hypothesis

Fig. 16. Axle deformation

Load 1 - forces and pressures p_1=68 MPa, p_2 = 100 MPa
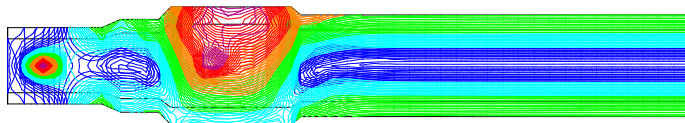
Equivalent stress [MPa]

```
1.33E+02 ... 1.60E+02
1.07E+02 ... 1.33E+02
8.00E+01 ... 1.07E+02
5.33E+01 ... 8.00E+01
2.67E+01 ... 5.33E+01
9.51E-04 ... 2.67E+01
```


Load 2 - forces and pressure p_1 = 68 MPa (p_2 = 0)

Equivalent stress [MPa]

```
1.32E+02 ... 1.58E+02
1.05E+02 ... 1.32E+02
7.90E+01 ... 1.05E+02
5.27E+01 ... 7.90E+01
2.63E+01 ... 5.27E+01
2.03E-03 ... 2.63E+01
```
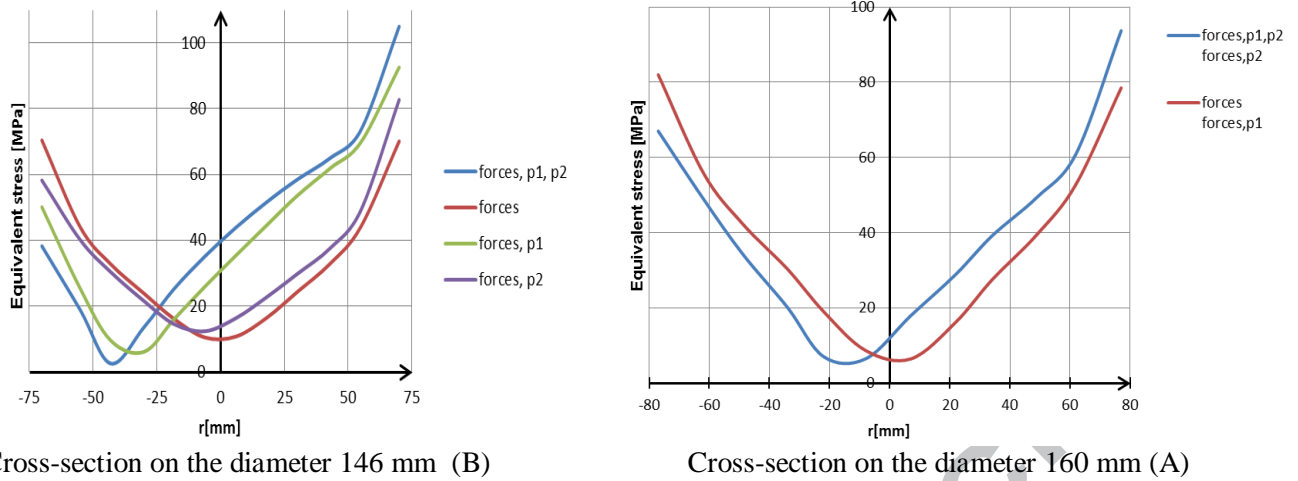

Load 3 - forces and pressure p_2 = 100 MPa (p_1 = 0)

Equivalent stress [MPa]

```
1.35E+02 ... 1.62E+02
1.08E+02 ... 1.35E+02
8.10E+01 ... 1.08E+02
5.40E+01 ... 8.10E+01
2.70E+01 ... 5.40E+01
1.86E-03 ... 2.70E+01
```

Fig. 17. Stress fields for different combinations of loads

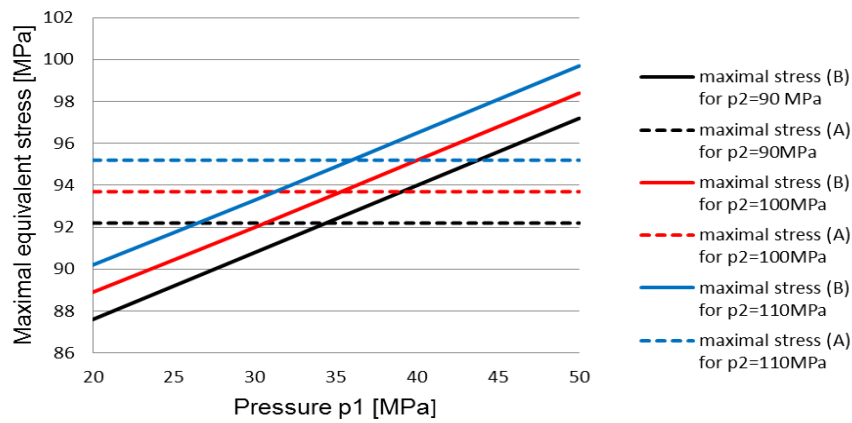Cross-section on the diameter 146 mm (B)   Cross-section on the diameter 160 mm (A)

Fig. 18. Diagrams of stress distribution in the observed cross-sections

Fig. 19. Maximal equivalent stress on positions (A) and (B) as a function of p_1

Table 1
Results of the axle material chemical analysis (mass. %)

Chemical element	C	Si	S	P	Mn	Ni	Cr	Mo	V	Ti	W	Al	Fe
	%	%	%	%	%	%	%	%	%	%	%	%	%
Sample 1 contents	0.441	0.260	0.005	0.009	0.640	0.034	0.097	0.012	< 0.003	< 0.003	0.020	0.069	rest
Sample 2 contents	0.438	0.268	0.005	0.009	0.640	0.034	0.099	0.012	< 0.003	< 0.003	0.020	0.071	rest
Specified according to EN 13261:2003	max. 0.40	max. 0.50	max. 0.020	max. 0.020	max. 1.20	max. 0.30	max. 0.30	max. 0.08	max. 0.06	-	-	-	
Specified according to SRPS P.F2.310	ND	max. 0.50	max. 0.05	max. 0.05	max. 1.20	max. 0.20	max. 0.30	max. 0.05	max. 0.05				

Table 2
Results of material mechanical properties testing

Test specimens position	Yield stress R_e (MPa)	Tensile strength R_m (MPa)	Elongation A_5 (%)	Contraction Z (%)
Longitudinal – surface	257	542	30.00	52.73
	253	533	29.50	52.73
Longitudinal – mid-radius	225	540	30.75	51.00
	222	522	32.50	51.00
Longitudinal - center	219	529	30.00	51.00
	219	535	31.50	51.00
Transverse	231	516	15.50	16.73
	235	529	17.00	19.00
Specified by EN 13261:2003 for longitudinal test specimens at mid-radius:	min 320	550 - 650	min 22	/
Specified by SRPS P.F2.310 for longitudinal test specimens:	/	550 - 630	/	/

Table 3
Measured impact energy

Test specimens position	Test temp. T(°C)	No.	Impact energy $KU_{5/300}$ (J)	Middle value $KU_{5/300}$ (J)
Longitudinal – surface	+ 20	1/2/3	21.58 / 21.58 / 21.58	21.58
Longitudinal – mid-radius	+ 20	1/2/3	21.58 / 20.60 / 16.68	19.62
Longitudinal - center	+ 20	1/2/3	24.53 / 25.51 / 22.56	24.20
Transverse - surface	+ 20	1/2/3	12.75 / 9.81 / 12.75	11.77
Transverse – mid-radius	+ 20	1/2/3	10.79 / 10.79 / 10.79	10.79
Transverse - center	+ 20	1/2/3	9.81 / 11.77 / 12.75	11.44
Specified by EN 13261:2003 for mid-radius in longitudinal / transverse direction			min. 30 J/ min. 25 J	

Table 4
Measured material hardness

Measuring position	Measured hardness (HBW)	Middle value (HBW)
Surface	146 – 148 - 149	148
Mid-radius	145 – 145 - 144	145
Center	143 – 145 - 143	144

Highlights

- Causes of railway axle fracture are obtained by numerical and experimental analysis.
- NDT had revealed surface cracks and corrosion pits in fracture zone.
- Destructive test results had shown degradation of the axle properties.
- The influence of press fit joints is of crucial importance for the analysis.
- Press fit of labyrinth seal and railway axle greatly affected to axle stress state.